Bulk Metallic Glasses, Synthesis, Thermal and Mechanical Characterizations

Jean-Louis Soubeyroux, Jean-Jacques Blandin, Marc Bletry, Pierre Guyot, Jean-Marc Pelletier

Bulk Metallic Glasses, Synthesis, Thermal and Mechanical Characterizations.

Jean-Louis Soubeyroux
Laboratoire de Cristallographie / CRETA / CNRS, 25 avenue des Martyrs, 38042 GRENOBLE Cedex, France
J.J. Blandin
GPM2/INP de Grenoble, 961 rue de la Houille Blanche, BP 46, 38402 Saint-Martin d'Hères, France
M. Blétry, P. Guyot
LTPCM/INP de Grenoble, 1130 rue de la Piscine, BP 75, 38402 Saint-Martin d'Hères, France
J.M. Pelletier
GEMPPM, INSA de Lyon, Bat. B Pascal, 69621 Villeurbanne, France

Abstract

The synthesis, the thermal and mechanical properties of new bulk metallic glasses are presented. The systems Zr-Ti-Cu-Ni-Al, Zr-Ti-Cu-Ni-Be and Mg-Cu-RE have drawn our particular attention due to the possibilities of applications in various fields. Synthesis is mainly done by HF melting and quenching in cooled copper moulds of various shapes (cylinders, plates, cones). Characterizations are done by X-ray and neutron diffraction, electron microscopies and differential scanning calorimetry techniques. The in situ powder neutron diffraction has been demonstrated as a powerful technique for the determination of the different phases appearing during crystallization. Mechanical properties have been determined by compression tests as a function of temperature. The effects of partial nanocrystallization and of a composite phase are investigated.

Introduction

The last ten years have seen the discovery of amorphous metal alloys that are glass forming at cooling rates as slow as 1°C s^{-1} to 100°C s^{-1} in the bulk via conventional metal processing such as casting, but with the ease of molding of polymers. They are twice as strong as steel, have greater wear and corrosion resistance, are tougher than ceramics, and yet have greater elasticity. Increased plasticity in amorphous/crystalline composites has been observed in several families.

The main systems studied for applications are Zr-TM-Al [], Zr-TM-Be [], Mg-TM-RE (TM=transition metal, RE=rare earth metal)[], Nb-Ni-Sn [], and others such as La-, Pd-, Fe-, Cu-, and Ti-based alloys with large under cooling and low critical cooling rates of 1°C

s-1 to 100°C s^{-1}, similar to oxide glasses. All these systems have in common several components (more than 3), they are constituted of elements that present an important size difference (of the order of 12%) and they form eutectic compositions in the binaries and ternaries phase diagrams. These observations have led to empiric rules for the choice of elements to mix to obtain bulk metallic glasses []. These alloys have in common several properties, in differential scanning calorimetry, they show before crystallization, an endothermic reaction that can be related to the glass transition observed in oxide glasses; they present a diffraction diagram of amorphous nature with a liquid-like appearance; they have high hardness compared to the crystallized alloy of the same family; their mechanical properties in the vicinity of the glass temperature are those of soft polymers.

In this study we will present some results on the Zr-TM-Al, Zr-TM-Be and Mg-TM-Gd systems that are the systems yet used in applications or will be used in a close future.

Experimental

Sample synthesis

Amorphous samples were prepared from a mixture of the pure elements by induction melting in a water-cooled copper crucible in argon/helium atmosphere. The zirconium provided by the CEZUS society was purified by heating under secondary vacuum at 1000°C. All the other alloys used have purity better than 99.5 %.

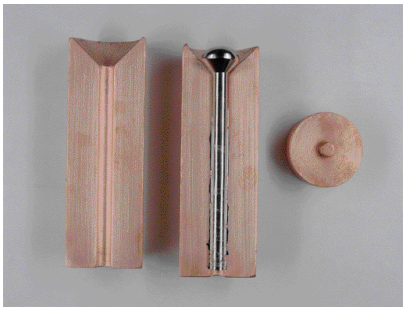

Figure 1: A 6 mm diameter alloy presented in a 3 pieces copper mould.

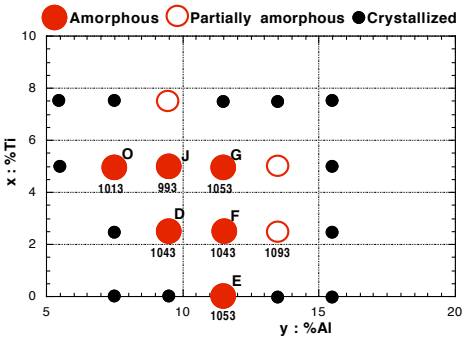

Figure 2: Composition dependence of the as-cast alloys for the $Zr_{65-x-y}Ti_xAl_yCu_{22}Ni_{13}$ system.

The ingots were melted by electromagnetic levitation and dropped into water-cooled copper mold of cylindrical shape of diameter 6 mm as represented in figure 1. Several rods were prepared from the same batch in order to perform the DSC and neutron diffraction experiments. For the Zr-TM-Al alloys, compositions were studied with generalized formulas: $Zr_{70-x-y}Ti_xAl_yCu_{19}Ni_{11}$, $Zr_{65-x-y}Ti_xAl_yCu_{22}Ni_{13}$, $Zr_{60-x-y}Ti_xAl_yCu_{25}Ni_{15}$ and general results are presented like in figure 2, where the alloys obtained as BMG are represented with large full circles, the alloys presenting a mixture of BMG and crystallized parts as large open circles and the alloys obtained crystallized as small circles (the letters above the circle stands for the given name to the alloy, the value under the circle stands for the

melting temperature. For the Zr-TM-Be alloys, compositions prepared were those reported by W.L. Johnson for the Vitreloy1 (ZrTiCuNiBe) and Vitreloy4 (ZrTiCuNiBe) alloys. For the Mg-TM-RE alloys, we have studied the $Mg_{65}Cu_{25}RE_{10}$ alloys with amorphous compounds obtained for RE=Y,Gd,Tb and Yb and crystallized samples for the other rare earth metals. Substitutions of Ni or Ag on the Mg or TM have also been studied. The compositions of the BMG presented in this study are given in table I.

Alloy Name	Zr	Ti	Cu	Ni	Al	Be
J35	50.0	5.0	22.0	13.0	10.0	
D35	52.5	2.5	22.0	13.0	10.0	
Vit1	41.2	13.8	12.5	10.0		22.5
Vit4	46.8	8.2	7.5	10.0		27.5

Table 1: Alloys compositions of the main alloys presented in this paper.

Sample characterization

The endothermic and exothermic reactions associated with glass transition and crystallization process were examined by differential scanning calorimetry (DSC) at different heating rates on a Netzsch DSC 404S calorimeter under a flowing argon atmosphere. Thermal events are characterized by a first endothermic reaction, whose temperature is determined by the inflexion point called T_{g2}; T_{g1} is the beginning of the event, T_{g3} the end. T_{x1} is the first exothermic event. T_f is the end of the endothermic melting event. ΔT is the temperature difference between T_{x1} and T_{g2}: $\Delta T=T_{x1}-T_{g2}$ (some authors use T_{g1} as parameter in this formula). Another parameter used to compare the glass forming ability of the BMG is γ, defined as $\gamma = \frac{T_l}{T_x - T_g}[]$. The lower γ value leading to the best ability to form bulk metallic glasses.

Characterization of the local composition was carried out by X-ray fluorescence analysis using a Kevex EDX probe attached to a JEOL 840 scanning electron microscope (SEM). Neutron diffraction experiments were performed on the D1B diffractometer of ILL-Grenoble which is equipped with a 400 cells position sensitive detector, covering an 80° 2-theta range, and allowing recording a pattern every 5 minutes. The wavelength used was 2.524Å. Mechanical properties at high temperature were investigated in compression, in air. The cylindrical samples were heated to a given test temperature at the same rate of 10 K/min as used in DSC. In order to get information about the rheology of the alloys, both strain rate jumps and tests at constant strain rate were carried out. The investigated temperature domain was from 340°C to 430°C whereas the strain rate interval was from $2.5x10^{-4}$ to $5x10^{-3}$ s^{-1}. From the measured flow stresses (for given strain rates), viscosities η were calculated according to $\eta = \sigma / 3\dot{\varepsilon}$.

Results

All X-ray diffraction patterns show the same liquid-like bumps that characterize the amorphous state and will not be presented here. DSC measurements reported in figures 3 to 7 are very different for all the studied compounds. The critical events are dependent of

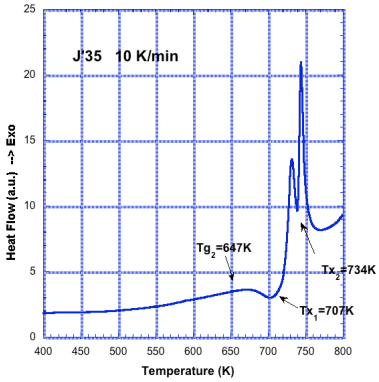

Figure 3: DSC trace for the J35 alloy.

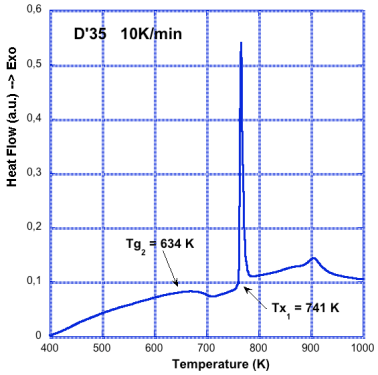

Figure 4: DSC trace for the D35 alloy.

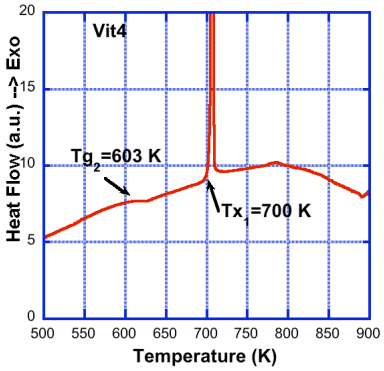

Figure 5: DSC trace for the Vit4 alloy.

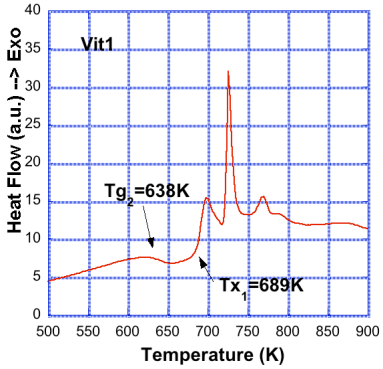

Figure 6: DSC trace for the Vit1 alloy.

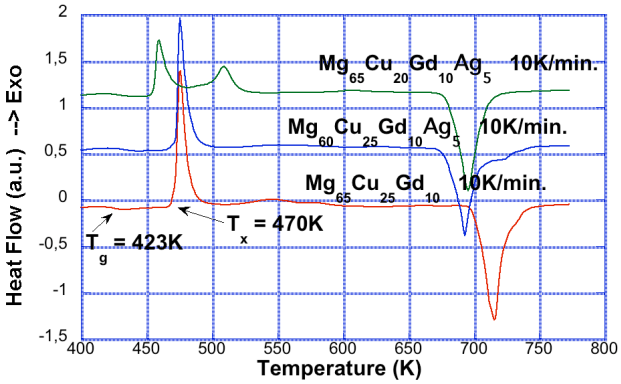

Figure 7: DSC trace for the $Mg_{65-x}Cu_{25-y}Gd_{10}$ alloys.

the measurement heating rate, Figures 3,4 and 7 have been recorded at 10K/min and figures 5 and 6 at 2K/min in order to be compared at the in-situ neutron experiments performed at the same heating rate. For some alloys such as D35, Vit4 and $Mg_{65}Cu_{25}Gd_{10}$ the DSC traces present a single important crystallization peak, with less important events at higher temperature. On the contrary, alloys J35, Vit1 and $Mg_{65}Cu_{20}Ag_5Gd_{10}$ present several peaks after the endothermic temperature event (T_g) that reduce the value of ΔT.

The results of the main temperature events observed in these figures are given in table II, they show that the D35 and Vit4 alloys present the best ability to produce BMG.

Alloy name	T_g (K)	T_x (K)	T_f (K)	ΔT	γ
J'35	647	707	1091	60	18.2
D'35	634	741	1036	107	9.7
Vit 1	638	689	1003	51	19.7
Vit 4	603	700	1185	97	12.2
$Mg_{65}Cu_{25}Gd_{10}$	423	470	733	47	15.6

Table II: Critical temperatures measured by DSC.

It is possible to study crystallization of the BMG by performing isothermal scans as a function of time in the vicinity of T_g. Figure 8 shows such an experiment for the D35 alloy.

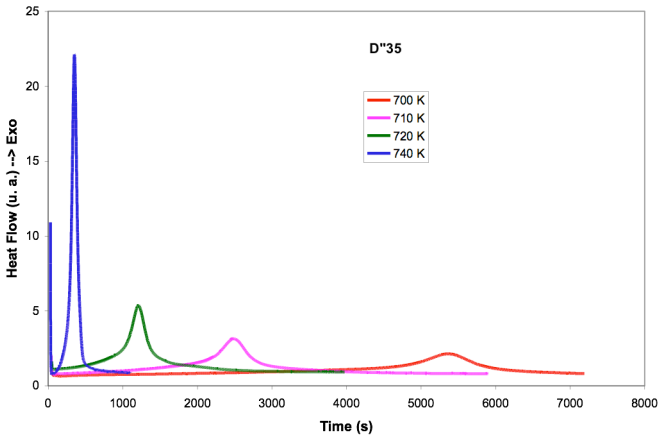

Figure 8: Isothermal DSC measurement for the D35 alloy.

The area under the crystallization peak can be related to the crystallized fraction (C) and fitted with the Johnson-Mehl-Avrami (JMA) equation (1):

$$\ln\left(\frac{\alpha}{T_p^2}\right) = \ln C - \frac{E}{RT_p} \quad (1)$$

where E is the activation energy, α the speed of heating and T_p the temperature of the peak. The crystallized fractions C measured at different temperatures as a function of time for the previous experiment are reported in figure 9. The fit with the JMA equation was done for the 710K temperature. A good agreement is obtained and allows determining the time necessary to anneal a sample at a given temperature to control the crystallized fraction.

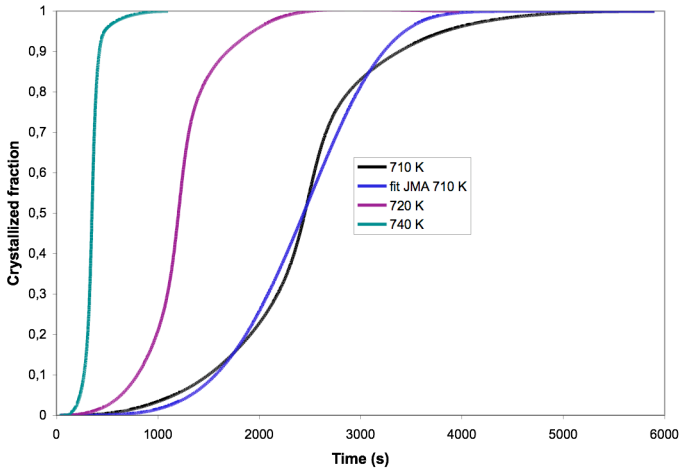

Figure 9: Crystallized fractions of the D35 sample at different temperatures in the ΔT interval, and the JMA fit at the 710K temperature.

Neutron diffraction experiments have been performed at the same heating rate than the DSC experiments. It is to note that neutron diffraction is a technique that analyses the sample in transmission and that all the volume of the sample diffracts. We have performed two kinds of experiments, the first one called “fast heating” is done continuously at 2°/min, the second one called “slow heating” is performed between room temperature and T_{g1} at 2°/min, then a plateau temperature of 120 minutes is done at this constant temperature, then a second and a third plateau of 120 minutes are done at T_{g1}+30° and T_{g1}+60°, up to the crystallization temperature, then the heating rate of 2°/min is continued until full crystallization.

The three-dimensional plot of figure 10 shows the diffraction diagrams registered every 5 minutes for the D35 sample. The sample shows at the beginning the liquid-like diagram of an amorphous alloy. Then at 736K new lines appear that can be attributed to binary compounds such as the tetragonal Zr_2Cu phase as the main compound and other phases noted on figure 10. A second crystallization appears at T_{x2} = 893K corresponding to the cubic Ti_2Ni phase. These temperatures can be related to the exothermic peaks observed in the DSC experiment performed at the same heating rate.

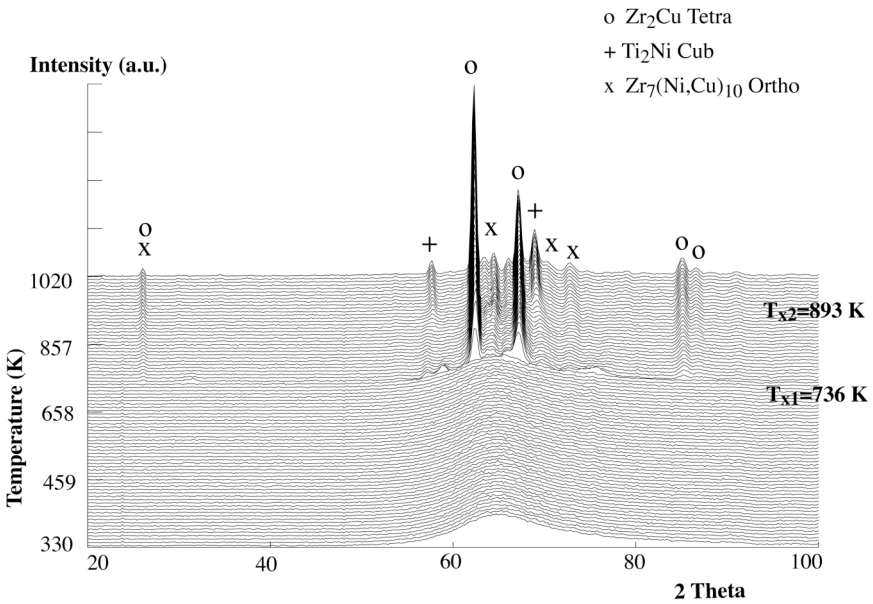

Figure 10: Thermodiffraction plot of a D35 sample with the fast heating rate.

The three-dimensional plot of figure 11 shows the diffraction diagrams registered for the "slow heating" mode for the D35 sample. The sample shows at the beginning the same liquid-like diagram, then at 693K a crystallization appears with the formation of a phase identified as the tetragonal Zr_2Ni phase, not observed in the fast experiment. This corresponds to Tg+60° in the DSC experiment. This phase is metastable and decomposes at 773K to form the tetragonal Zr_2Cu phase. At higher temperature (874K) the phases observed in the previous experiment are also observed. So, during annealing in the ΔT region, the phases formed are different than the phases formed during the fast heating process. But after this phase recombination the stability of the other phases is the same and the final phases obtained at the end of the crystallization process are the same.

The three-dimensional plot of figure 12 shows the diffraction diagrams registered for the "fast heating" mode for the Vit4 sample. As previously, the diagram presents the liquid-like diagram, then at T_{x1}=655K a series of diffraction peaks appear in an interval of temperature of 5° with a fully crystallized sample. No other new peaks are observed up to 900K. This crystallization temperature is in accordance with the single crystallization event observed in the DSC trace. Several phases are formed, among them Zr_2Cu and Zr_2Ni have been identified.

The three-dimensional plot of figure 13 shows the diffraction diagrams registered for the "slow heating" mode for the Vit4 sample. During the plateau temperature at 630K, and after 1 hour of annealing, new peaks appear and increase in intensity with time. During the second temperature plateau at 650K, and after 10 minutes, the first phase decomposes and new peaks appear.

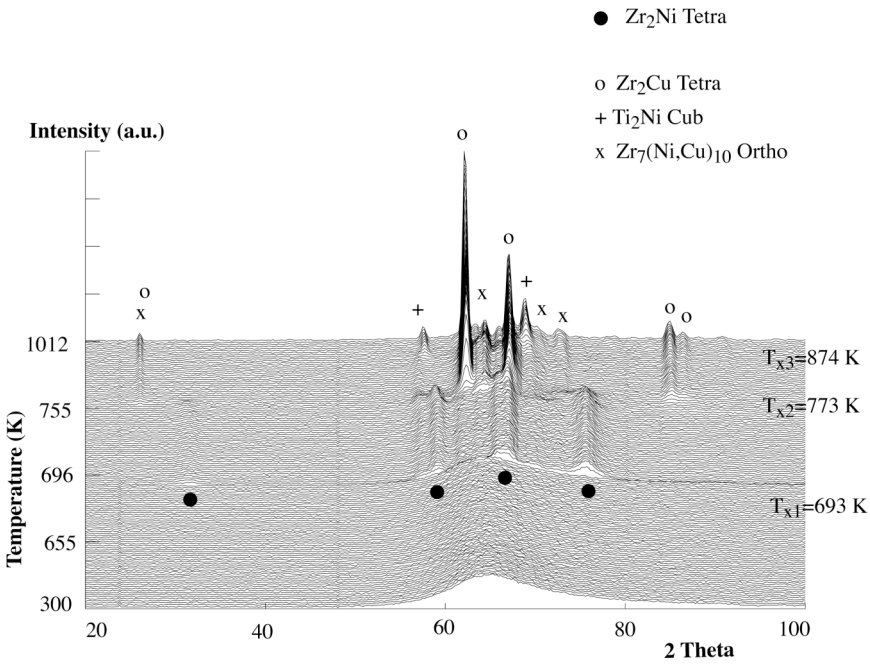

Figure 11: Thermodiffraction plot of a D35 sample with the slow heating rate.

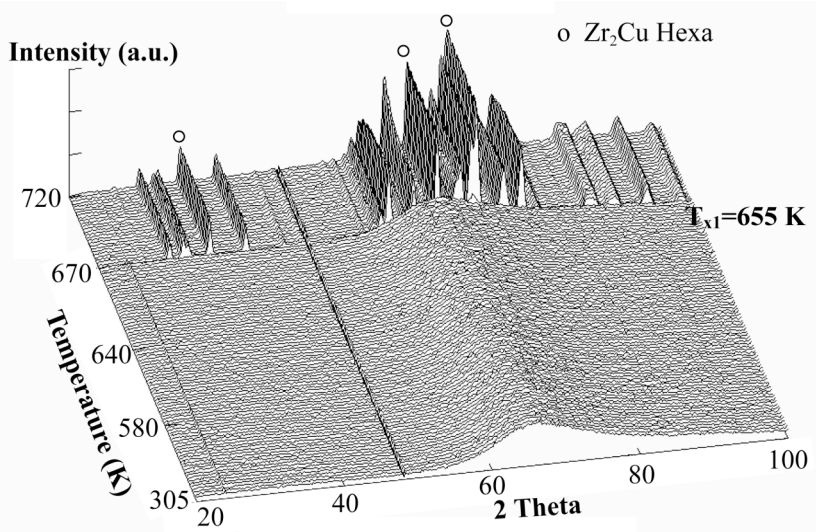

Figure 12: Thermodiffraction plot of a Vit4 sample with the fast heating rate.

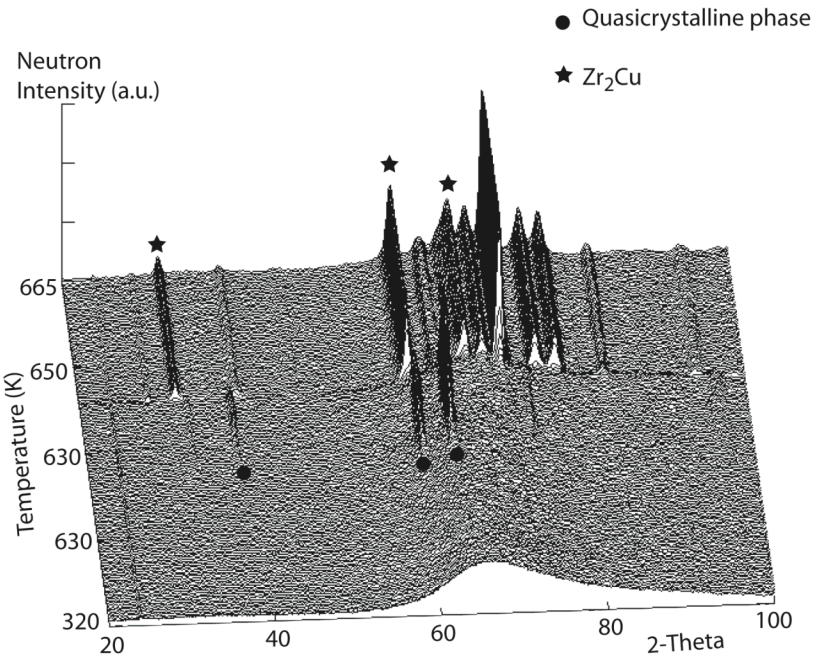

Figure 13: Thermodiffraction plot of a Vit4 sample with the slow heating rate.

The final peaks are the same as in the previous experiment, with Zr_2Cu and Zr_2Ni as the main phases. However the new peaks have been identified as quasicrystal lines, identified later as a quasicrystal phase beryllium free, that crystallizes simultaneously with $ZrBe_2$, not evidenced in this experiment, but in X-ray diffraction patterns recorded an annealed and quenched samples [xx]. This observation is in accordance with isothermal DSC experiments performed on the same compound, but full crystallization was obtained after 6 hours.

A similar experiment, not represented here, has been performed on the vit1 sample that presents several crystallization events during the DSC experiment. During the "fast heating" experiment, binary phases are formed in accordance with the temperatures observed in DSC, but during the "slow heating", during annealing at T_{g2}, an amorphous phase separation appears, and in the diffraction pattern, two new maxima of the main bump are clearly observed. To analyze the compositions of these new phases, several techniques will be used.

Figures 14 and 15 show typical stress-strain curves obtained during a constant strain rate test performed on the D35 and J35 samples, respectively, at different temperatures in the vicinity of Tg. On the D35 sample, a stress plateau is quickly reached at all temperatures and consequently there is no difficulty to deform the sample. For the J35 sample, at the higher temperature (703K), the stress necessary to deform the sample increases. After deformation the X-ray analysis has shown that crystallization occurs in this sample.

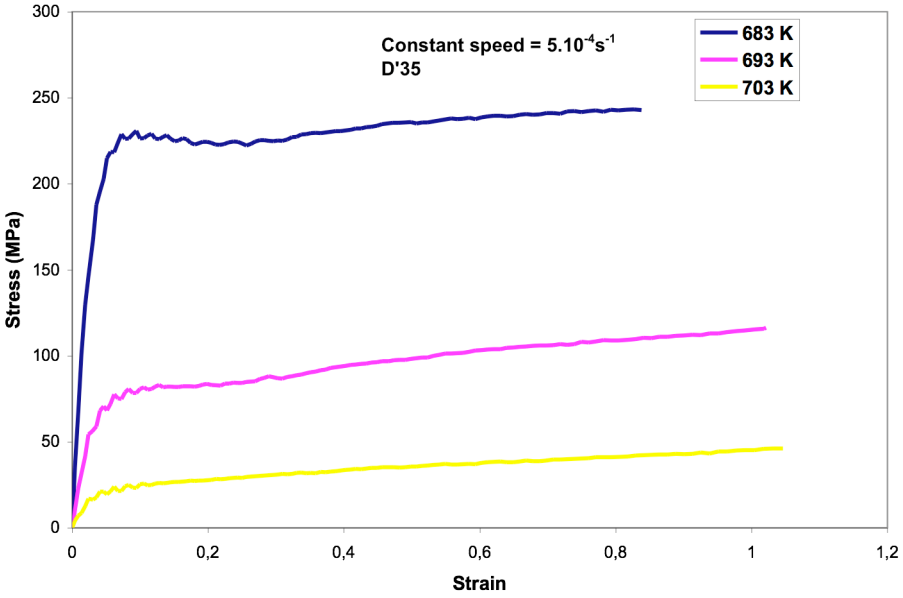

Figure 14: Hot deformation of the D35 sample at constant deformation speed (5.10^{-4} s^{-1}).

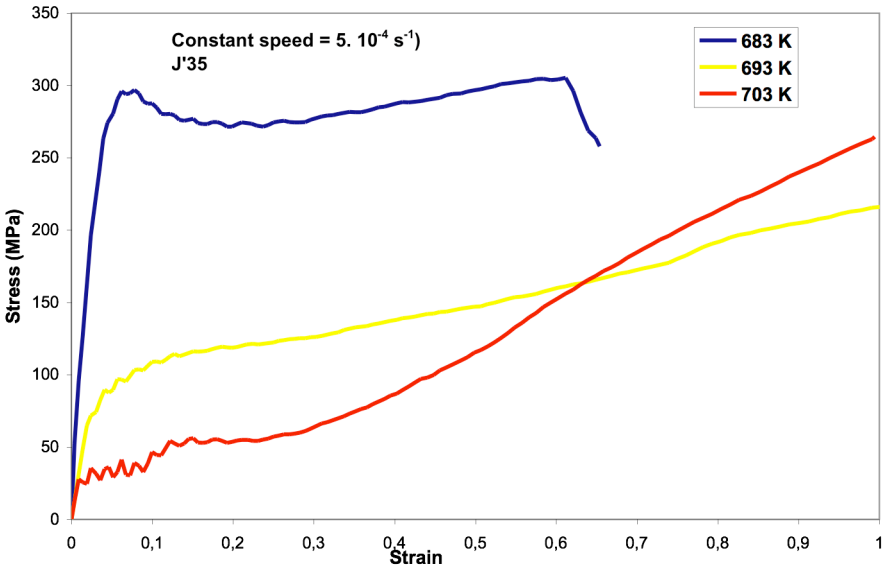

Figure 15: Hot deformation of the J35 sample at constant deformation speed (5.10^{-4} s^{-1}).

Figure 16 shows a typical stress-strain curve obtained during a strain rate jump test performed on the D35 sample, at 693K. At low strain rates, a stress plateau is quickly reached and consequently there is no difficulty to measure an apparent equilibrium viscosity. For high stresses, slight stress overshoots are detected. However a comparison of two experiments, one performed with stress-strain jumps and the other at constant speed show the same level of stress after deformation.

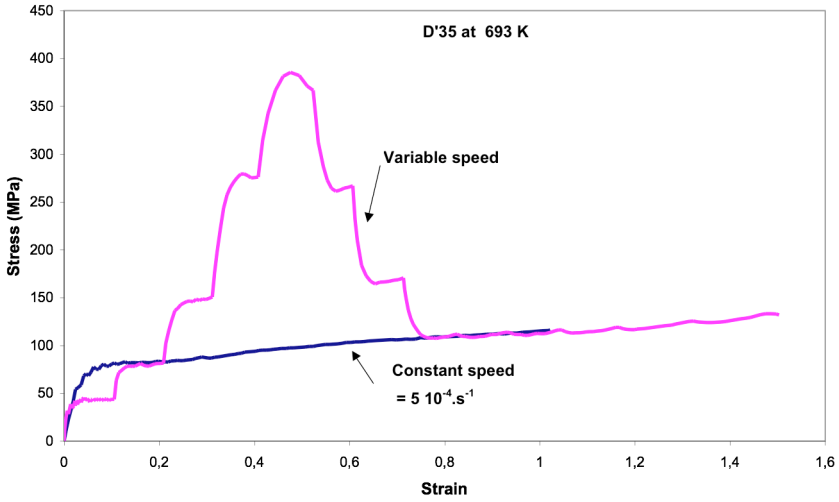

Figure 16: Stress-strain curve obtained during a strain rate jump test at 693K (D35).

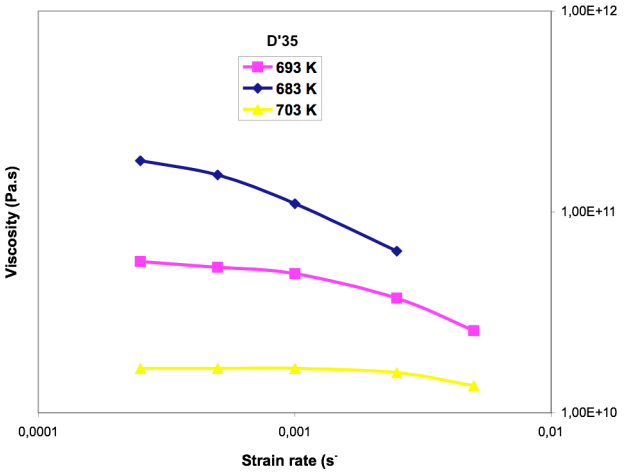

Figure 17: Viscosity *vs.* strain rate at various temperatures for the D35 alloy.

Figure 17 displays the effect of both temperature and strain rate on apparent equilibrium viscosities in the case of the D35 alloy. At 703K, a nearly Newtonian behaviour is obtained with an apparent viscosity close to 10^{10} Pa.s is measured. As far as temperature is reduced, the Newtonian behaviour is obtained for lower strain rates.

Figure 18 shows the stress-strain curve measured on the MgCuGd sample at room temperature. The value of 700 MPa reached for the stress is the most important one obtained for a magnesium alloy. However, no plastic deformation appears and the sample breaks in many parts at the rupture point.

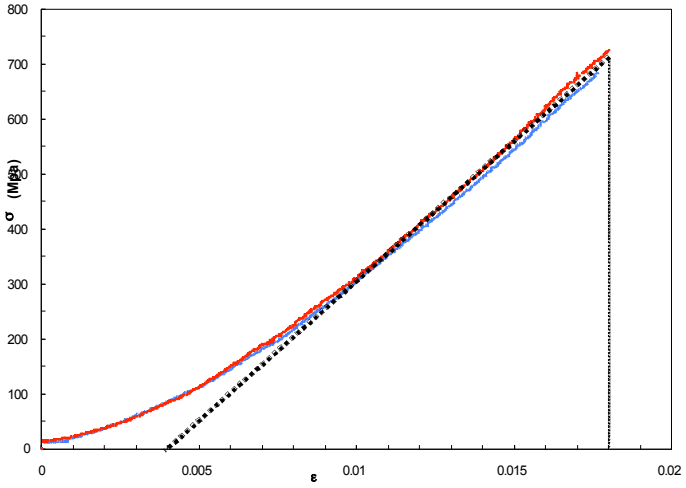

Figure 18: Stress-strain curve for the $Mg_{65}Cu_{25}Gd_{10}$ sample at 300K.

To overpass this behaviour, we have prepared composite samples with compositions $(Mg_{65}Cu_{25}Gd_{10})_{100-x}Fe_x$ ($3 \leq x \leq 12$). By X-ray diffraction the samples show an amorphous bump superimposed to α-Fe lines, showing that composite samples have been formed. The DSC trace reported in figure 19 for the x=3 sample shows that the curves present the same behaviour, indicating that the amorphous matrix has not been changed by the iron. The stress-strain curve obtained for this composite sample, figure 20, shows a stress increase to 800Mpa, and a beginning of plasticity, but further experiments are needed on the other samples with a higher iron content.

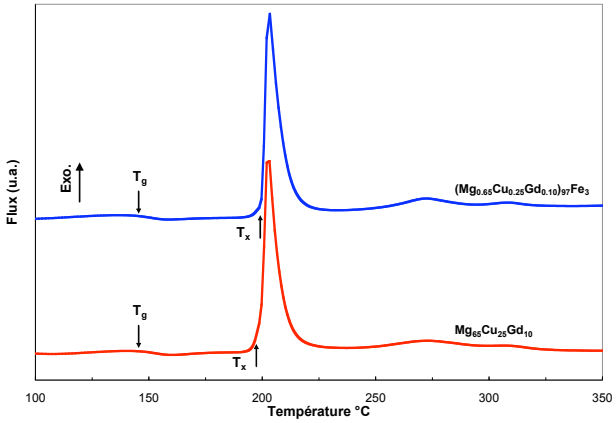

Figure 19: DSC traces of the $Mg_{65}Cu_{25}Gd_{10}$ and $(Mg_{65}Cu_{25}Gd_{10})_{97}Fe_3$ samples.

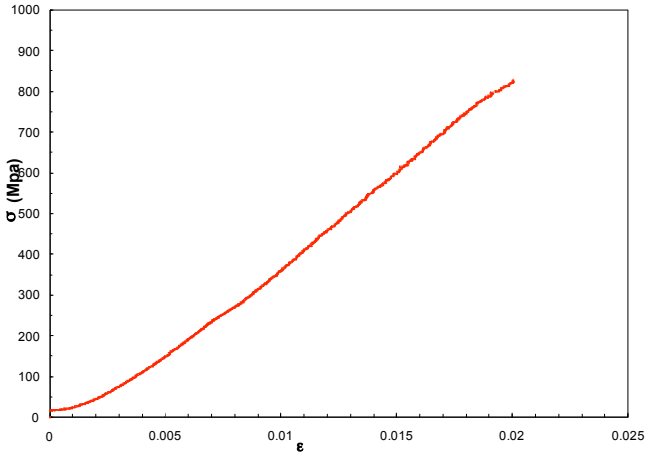

Figure 20: Stress-strain curve of the and $(Mg_{65}Cu_{25}Gd_{10})_{97}Fe_3$ samples at 300K.

Conclusion

Bulk metallic glasses with a lower dimension of several millimeters can be prepared by mould casting techniques from a judicious choice of the metals taking into account the atomic size difference, the formation enthalpy and the vicinity of eutectics in the binary alloys. To characterize the BMG, the DSC curves are a fruitful tool to get information on the characteristic temperatures and to the glass forming ability criteria defines by several

authors. In-situ powder neutron diffraction has allowed us to obtained direct information between the events observed by DSC and the crystallization of the samples. In particular isothermal scans have revealed crystallization of phases different of the constant speed scans. For the vitreloy4 sample a quasicrystal phase has been demonstrated to be present at the same time than $ZrBe_2$. This behavior shows that the mobile clusters near the glass transition temperature contain this entity and that the icosahedral stable clusters are formed with Zr, Ti, Cu and Ni elements.

Among the different phases formed, alloys with a unique crystallization temperature present larger temperature range for deformation and must be preferred to multiple crystallization alloys. Temperature ranges of 100 degrees have been obtained on the Vit4 and D35 samples.

References

[1] A. Inoue, T. Zhang, T. Matsumoto, Mater. Trans. JIM 31 (1990), p. 177.
[2] A. Peker, W.L. Johnson, Appl. Phys. Lett. 63 (1993), p. 2342.
[1] W.L. Johnson, Mater. Sci. Forum 225-227 (1996) 35 ; MRS Bull. 24 (1999) 42
[3] R. Rambousky, M. Moske, K. Samwer, Mater. Sci. Forum 170-181 (1995), p. 761.
[4] L.Q. Xing, J. Eckert, W. Löser, L. Schultz, D.M. Herlach, Phil. Mag. A 79 (1999), p. 1095.
[5] J.M. Pelletier, Y. Jacquemard, J. Perez, R. Perrier de la Bâthie, MRS Symposium Proceedings, vol 554, (1998), p. 413.
[7] J.L.Soubeyroux, J.M. Pelletier, R. Perrier de la Bâthie, Physica B 276-278 (2000), p. 905.
[8] J. Eckert, N. Mattern, M.Zinkevitch, M. Seidel, Mater. Trans. JIM 39 (1998), p.623.
[9] K.F. Kelton, W.J. Kim, R.M. Stroud, Appl. Phys. Lett. 70(24) (1997) p. 3230.
K. Amiya and A. Inoue. Thermal stability and mechanical properties of Mg-Y-Cu-M (M=Ag, Pd) bulk amorphous alloys. Materials Transactions, JIM, Vol. 41 No11 (2000) pp1460-1462.
K. Amiya and A. Inoue. Preparation of bulk glassy $Mg_{65}Y_{10}Cu_{15}Ag_5Pd_5$ alloy of 12mm in diameter by water quenching. Materials Transactions, JIM, Vol. 42 No3 (2001) pp543-545.
H. Men and D.H. Kim. Fabrication of ternary Mg–Cu–Gd bulk metallic glass with high glass-forming ability under air atmosphere. J. Mater. Res., Vol. 18, No. 7, Jul 2003.